Wave-Vector-Varying Pancharatnam-Berry Phase Photonic Spin Hall Effect

Wenguo Zhu[1,*] Huadan Zheng,[1] Yongchun Zhong,[2] Jianhui Yu,[2,†] and Zhe Chen[2]

[1]*Guangdong Provincial Key Laboratory of Optical Fiber Sensing and Communications, Jinan University, Guangzhou 510632, China*
[2]*Key Laboratory of Optoelectronic Information and Sensing Technologies of Guangdong Higher Education Institutes, Department of Optoelectronic Engineering, Jinan University, Guangzhou 510632, China*

The geometric Pancharatnam-Berry (PB) phase not only is of physical interest but also has wide applications ranging from condensed-matter physics to photonics. Space-varying PB phases based on inhomogeneously anisotropic media have previously been used effectively for spin photon manipulation. Here we demonstrate a novel wave-vector-varying PB phase that arises naturally in the transmission and reflection processes in homogeneous media for paraxial beams with small incident angles. The eigenpolarization states of the transmission and reflection processes are determined by the local wave vectors of the incident beam. The small incident angle breaks the rotational symmetry and induces a PB phase that varies linearly with the transverse wave vector, resulting in the photonic spin Hall effect (PSHE). This new PSHE can address the contradiction between spin separation and energy efficiency in the conventional PSHE associated with the Rytov-Vladimirskii-Berry phase, allowing spin photons to be separated completely with a spin separation up to 2.2 times beam waist and a highest energy efficiency of 86%. The spin separation dynamics is visualized by wave coupling equations in a uniaxial crystal, where the centroid positions of the spin photons can be doubled due to the conservation of the angular momentum. Our findings can greatly deepen the understanding in the geometric phase and spin-orbit coupling, paving the way for practical applications of the PSHE.

The geometric phase, which arises when a classical or quantum system undergoes a cyclic and adiabatic evolution in its parameter space [1], is of primary importance in modern physics [2,3]. Obviously different from its dynamic counterpart, the geometry phase depends on the shape of the path that is taken. In optics, there are mainly two types of geometric phase: Rytov-Vladimirskii-Berry (RVB) [3] and Pancharatnam-Berry (PB) phases [4]. The former is associated with the evolution of the propagation direction of light, whereas the latter with the polarization evolution on the Poincaré sphere [1,5]. Spatially varying PB phases based on anisotropic media have been widely investigated, speeding up the development of integrated spin-photonic devices [6–11]. Inhomogeneous liquid crystals and metasurfaces are frequently employed to design functional PB optical elements with energy efficiencies as high as nearly 100% [9,12–14]. Spin photons can be manipulated flexibly in the momentum space by arranging the optical axes of the anisotropic unit cells. The manipulated spin photons could, thus, be observed at a distance after the PB elements.

The RVB phase occurs in nonparaxial light beams as well as paraxial beams in their reflection and transmission processes [15–18]. Because of the RVB phase, a linearly polarized light beam will undergo a transverse spin separation when reflected by or transmitted through a homogeneous interface, leading to the so-called photonic spin Hall effect (PSHE) [19]. This RVB phase is momentum dependent, and, thus, the spin separation occurs in the real space. The RVB phase is generally small and allows the spin separation of only a few tenths of wavelength, which is very difficult for observation [20]. Nevertheless, a horizontally polarized beam reflected near the Brewster angle can undergo a large spin separation [21]. However, the Fresnel reflection coefficient for p wave is near zero around the Brewster angle, and, hence, only a small part of the incident power will be reflected. To obtain a spin separation of 20λ (λ being the wavelength), the reflectivity is about -50 dB for an air-prism interface. Moreover, the larger the spin separation, the lower the reflectivity. This is because the reflectivity (energy efficiency) appears in the denominator in the expression for the spin separation [20,22]. Taking full advantage of this fact, large spin separations have been obtained with the assistance of lossy modes [23], surface plasmon resonances [24], and Dirac points [25] in the reflection scheme as well as of metamaterials [26] in the transmission scheme. However, all of these large separations are accompanied with a low energy efficiency [27]. Although the small spin separation can be amplified by weak measurement techniques, they suffer from the same problem of low energy efficiency [17,28]. Besides, the spin separation is accompanied with distortion in the beam intensity profile. It was demonstrated that there are upper limits for the spin separation [27,29,30], which must be smaller than the intensity spot size. For a Gaussian, the
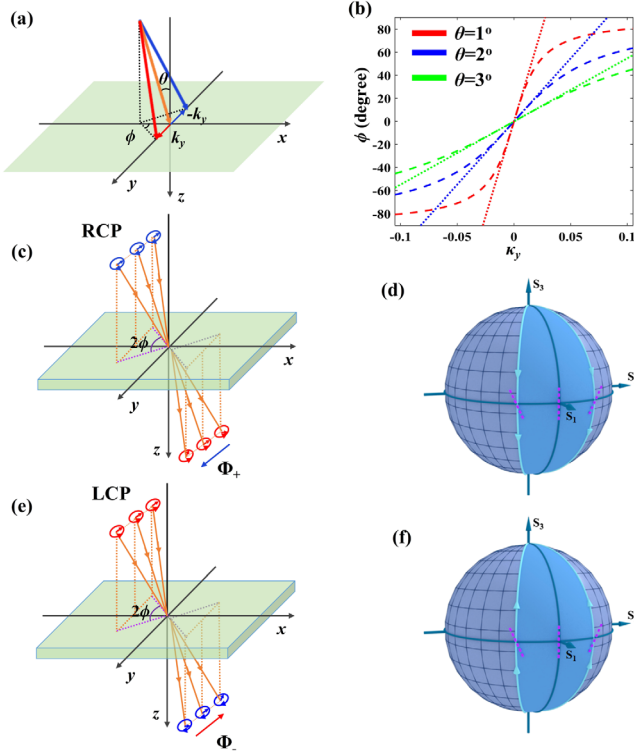
FIG. 1. (a) Schematic of the variation of the azimuthal angle ϕ with the transverse wave vector κ_y. (b) Exact nonlinear and approximately linear relations between ϕ and $\kappa_y H$. Right (c) and left (e) circular polarization states transmitting through a slab and acquiring spin flipping and opposite PB phase gradients. (d) and (f) illustrate the evolution of the polarization states on the Poincaré sphere. The cyan trajectories represent spin conversions through different local incident planes, corresponding to (c) and (e), respectively. Half of the solid angles encompassed by the cyan areas is the PB phase.

limit is the incident beam waist w_0 [31]. Owing to this upper limit, the spin photons are not fully separated. These facts severely restrict the practical applications of the PSHE.

Here, a novel PSHE is demonstrated with a giant spatial spin separation and a high energy efficiency based on a wave-vector-varying PB phase. We find that the wave-vector-varying PB phase is generated naturally in the reflection and transmission processes for paraxial beams with a small incident angle, where the polarization evolutions can be well described on the Poincaré sphere. The PB phase changes linearly with the transverse wave vector, allowing the spin photons to be separated completely with a high energy efficiency. Moreover, the spin-orbit coupling and spin separation processes within a uniaxial crystal are studied.

Assume that a paraxial light beam illuminates a spatially homogeneous medium with a small incident angle θ; the incident beam can be considered as a superposition of plane waves with different wave vectors. As shown in Fig. 1(a), the incident wave vectors k_y have a spread along

the y axis. The azimuthal angle of the local wave vector is given by [32]

$$\phi = \mathrm{atan}[\kappa_y/\sin\theta(1-\kappa_y^2)^{1/2}] \approx \kappa_y/\sin\theta, \qquad (1)$$

where $\kappa_y = k_y/k_0$ with k_0 being the wave number in vacuum. The local incident plane (azimuthal angle) increases linearly with κ_y when $\phi \ll 1$ for paraxial beams ($\kappa_y \ll 1$). Figure 1(b) presents the accurate and approximately linear relationships between ϕ and κ_y for incident angles of 1°, 2°, and 3°. It can be observed that, for a small incident angle, a small change of the transverse wave vector will cause a large rotation of the local incident plane. It is also worth noting that the incident angle is identically equal to θ regardless of the change of the local incident plane [32].

To reveal the physical principle of the wave-vector-varying PB phase, we assume an incident one-dimensional (1D) paraxial Gaussian beam with an angular spectrum of $\tilde{\mathbf{E}}_i = \tilde{u}_0[a|H\rangle + b|V\rangle]$, where a and b are the complex coefficients for horizontal (H) and vertical (V) polarization states, respectively, and the Gaussian profile is $\tilde{u}_0 = \exp[-k_y^2 w_0^2/4]$. The incident angular spectrum is first decomposed into a superposition of parallel (p) and perpendicular (s) plane waves prior to transmission, that is, transforming the incident beam from local coordinates to spherical global coordinates [20] with the transformation matrix given by $\hat{U} = \hat{R}_y(\theta)\hat{R}_z(\phi)\hat{R}_y(-\theta)$ [32]. When the incident angle is very small, the matrix has the simple form

$$\hat{U} = \begin{bmatrix} \cos\phi & \sin\phi \\ -\sin\phi & \cos\phi \end{bmatrix}. \qquad (2)$$

The transmitted angular spectrum is connected with the incident one by the transmission coefficients $\hat{F} = \mathrm{diag}[t_p, t_s]$ [20]. Under the paraxial approximation, t_p and t_s depend only on the incident angle [32]. The transmitted beam in local coordinates is therefore $\tilde{\mathbf{E}}_t = \hat{U}^+ \hat{F} \hat{U} \tilde{\mathbf{E}}_i$. In the circular polarization bases ($|\pm\rangle = |H\rangle \pm i|V\rangle$), the complete transformation matrix is in the form

$$\hat{T} = \begin{bmatrix} t_p + t_s & (t_p - t_s)\exp[-2i\kappa_y/\sin\theta] \\ (t_p - t_s)\exp[2i\kappa_y/\sin\theta] & t_p + t_s \end{bmatrix}. \qquad (3)$$

The wave-vector-varying PB phases are seen to be $\Phi_\pm = \pm 2\kappa_y/\sin\theta$. A right-circular polarization (RCP) state will then be transformed partially to a left-circular polarization (LCP) state acquiring a phase gradient of $2\kappa_y/\sin\theta$, while an incident LCP state will to a RCP state with $-2\kappa_y/\sin\theta$ [34], as shown in Figs. 1(c) and 1(e). The corresponding evolutions of the polarization states on the Poincaré sphere are illustrated in Figs. 1(d) and 1(f), respectively. The PB phases are associated with half of the

solid angles encompassed by the cyan areas. Hence, the wave-vector-varying PB phases will lead to spin separation in the real space. For H incident polarization, the spin-dependent displacements can be obtained in the ideal case of $t_p = -t_s = 1$ as [32]

$$\Delta_\pm = -\frac{\partial \Phi_\pm}{\partial(k_y)} = \mp \frac{\lambda}{\pi \sin \theta}. \quad (4)$$

A small incident angle can thus induce a giant spin separation ($\Delta = \Delta_+ - \Delta_-$). For $\theta = 1°$, the spin separation is up to 36.4λ. The giant spin separation does not necessarily induce energy loss. This is quite different from the conventional PSHE, where a large spin separation results directly from the small energy of the transmitted beam, as the energy appears in the denominator in the expression for spin-dependent separation [20,22]. Although based on the transmission process, the above derivation can be readily extended to the reflection process. The PSHE based on the wave-vector-varying PB phase can occur in different optical systems where the eigenpolarization states change with the wave vector, such as Gaussian beams reflected by an epsilon-near-zero metamaterial (demonstrated in Supplemental Material [32]) and transmitted through a uniaxial crystal.

When a Gaussian beam passes through a uniaxial crystal with its optical axis perpendicular to the interface, the transmitted field can be readily given via Eq. (3), which, however, cannot give the spin-orbit coupling detail within the crystal. To this end, we exploit the two wave coupling equations [32,35]:

$$2i\frac{\partial A_+}{\partial z} + \frac{\chi}{2k_0 n_o}\left[-(k_0 \sin\theta)^2 + \frac{\partial^2}{\partial y^2}\right]A_+$$
$$= \frac{\delta}{2k_0 n_o}\left[(k_0 \sin\theta) - \frac{\partial}{\partial y}\right]^2 A_-, \quad (5)$$

$$2i\frac{\partial A_-}{\partial z} + \frac{\chi}{2k_0 n_o}\left[-(k_0 \sin\theta)^2 + \frac{\partial^2}{\partial y^2}\right]A_-$$
$$= \frac{\delta}{2k_0 n_o}\left[(k_0 \sin\theta) + \frac{\partial}{\partial y}\right]^2 A_+, \quad (6)$$

where $\mathbf{A} = A_+|+\rangle + A_-|-\rangle$ is the slowly varying amplitude, $\chi = n_o^2/n_e^2 + 1$, and $\delta = n_o^2/n_e^2 - 1$ with $n_{o,e}$ being the refractive indies of the ordinary (o) and extraordinary (e) waves, respectively. The RCP and LCP components (A_+ and A_-) are coupled to each other as a consequence of the anisotropy δ. Interestingly, the coupling terms $\mp[\delta \sin\theta/2n_o]\partial_y A_\mp$ push the RCP and LCP components toward the $\pm y$ directions, resulting in the PSHE. With the initial field given by $\mathbf{E}_i = \exp[-y^2/w_0^2\sigma_0 + ixk_0\sin\theta]/w_0\sigma_0[a|H\rangle + b|V\rangle]$ with $\sigma_0 = 1 - 2i(z - L/n_o)/k_0w_0^2$ (L being the crystal length), the coupling equations can be solved numerically. The boundary condition (initial field) is directly given at the $z = 0$ plane without
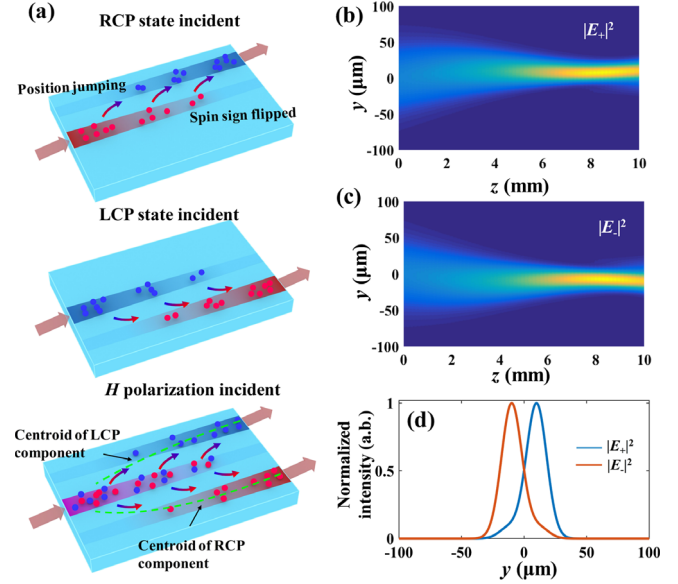

FIG. 2. (a) Schematics of spin photon separation in a uniaxial crystal for RCP, LCP, and H incident polarizations. Propagations of RCP (b) and LCP (c) components for H incident polarization. (d) Normalized intensity profiles at the output interface.

considering the interface effect. This is applicable when the input and output interfaces are coated with ideal antireflection films. Figures 2(b)–2(d) show the dynamic evolutions of the RCP and LCP components for H incident polarization.

A plane wave $\tilde{\mathbf{E}}_\perp = [E_+|+\rangle + E_-|-\rangle]\exp[i(k_x x + k_y y + k_z z)]$ propagating in a uniaxial crystal follows [32,36,37]:

$$\chi(k_x^2 + k_y^2)\mathbf{\Psi} + \delta(k_x^2 - k_y^2)\sigma_x\mathbf{\Psi} + 2\delta k_x k_y\sigma_y\mathbf{\Psi} = E\mathbf{\Psi}. \quad (7)$$

Since $k_x = k_0 \sin\theta$ is fixed, $2\delta k_x$ is the spin-orbit coupling parameter. Therefore, the small incident angle beaks the inversion symmetry of the system, which is somehow analogous to the applied electric field in Rashba-Dresselhaus spin-orbit coupling [36–38]. The eigenvectors are $\mathbf{\Psi} = (\pm e^{-2i\phi})|+\rangle + |-\rangle$ with eigenvalues of $E = (\chi \pm \delta)(k_x^2 + k_y^2)$, which correspond to $k_z^e = [k_0^2 n_e^2 - k_x^2 - k_y^2]^{1/2}n_o/n_e$ and $k_z^o = [k_0^2 n_o^2 - k_x^2 - k_y^2]^{1/2}$, respectively. For an RCP or LCP incident state, the light field in the crystal is $\tilde{\mathbf{E}}_\perp^\sigma = [e^{ik_z^e z} + e^{ik_z^o z}]|\sigma\rangle + [e^{ik_z^e z} - e^{ik_z^o z}]e^{2i\sigma k_y/\sin\theta}|-\sigma\rangle$ ($\sigma = \pm 1$). The spin sign of the second term is flipped, while that of the first term is kept. The spin conversion efficiency is $\eta = 0.5[1 - \cos(\delta k_0 z \sin^2\theta/2n_o)]$. At an arbitrary z plane, the intesnity centoid of the spin-unconverted photons are maintained at $y = 0$, while those of the converted photons are at $y = -\sigma\lambda/\pi \sin\theta$ for RCP and LCP incident states. These discrete and double-valued centroid positions of the spin photons are protected by the conservation of the total angular momentum [32]. For H incident polarization state, the centroid displacements of the spin components change
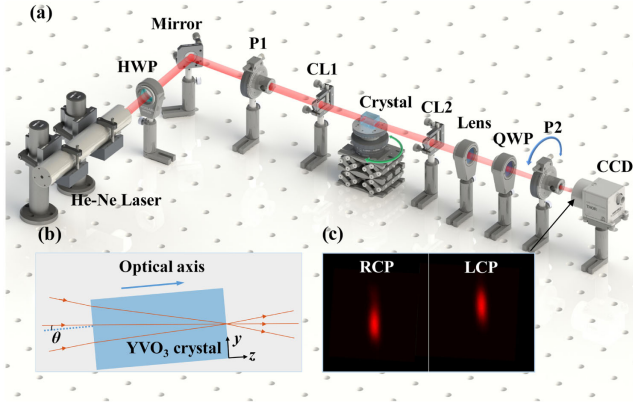
FIG. 3. Experimental demonstration of the PSHE based on the wave-vector-varying PB phase. (a) Experimental setup. (b) A paraxial light beam is focused obliquely into the YVO_3 crystal with the focal point at the output plane of the crystal. (c) CCD recorded RCP and LCP components of the transmitted beam, where a relative vertical displacement is obvious.

gradually with z, since they contain both spin-unconverted and spin-converted photons. The whole pictures of the PSHE process are illustrated in Fig. 2(a) for RCP, LCP, and H incident polarizations.

In the experimental setup shown in Fig. 3(a), a 632.8 nm Gaussian beam from a He-Ne laser passed through a half-wave plate (HWP) and was reflected by a mirror to a polarizer $P1$, which then made the beam H polarized. Next, a cylindrical lens (CL1) with a focal length of $f = 50$ mm focused the beam into a $4 \times 4 \times 10$ mm yttrium vanadate (YVO_3) crystal ($n_o = 2.2154$ and $n_e = 1.9929$) [39]. As indicated in Fig. 3(b), the focal point was at the output plane of the uniaxial crystal with an elliptical spot size of 550×15 μm at normal incidence. The incident angle could be tuned by precisely rotating the crystal. The transmitted light field at the output plane was imaged by a combination of a cylindrical lens CL2 ($f = 50$ mm), a spherical lens ($f = 250$ mm), and a CCD camera. With a quarter-wave plate (QWP) and polarizer $P2$, we could select the RCP or LCP component of the transmitted beam, as shown in Fig. 3(a).

The theoretical and experimental results of the displacements and energies of the two opposite-spin components of the transmitted beam are compared in Fig. 4, where good agreement is observed. The displacements oscillate with the incident angle owing to the oscillation of the phase difference between t_p and t_s, as illustrated in Fig. S1 in Supplemental Material [32]. Displacement peaks emerge at points with a 180° phase difference, and the peak values follow the prediction of Eq. (4), i.e., being inversely proportional to $|\sin\theta|$, except for the two central ones. It is worth noting that the spin separation at $\theta = \pm1.40°$ could reach $|\Delta| = 18.2$ μm, which is $1.21w_0$ and exceeds the upper limit in the conventional PSHE [22,24,25]. The obtained large spin separation here is accompanied with a high energy
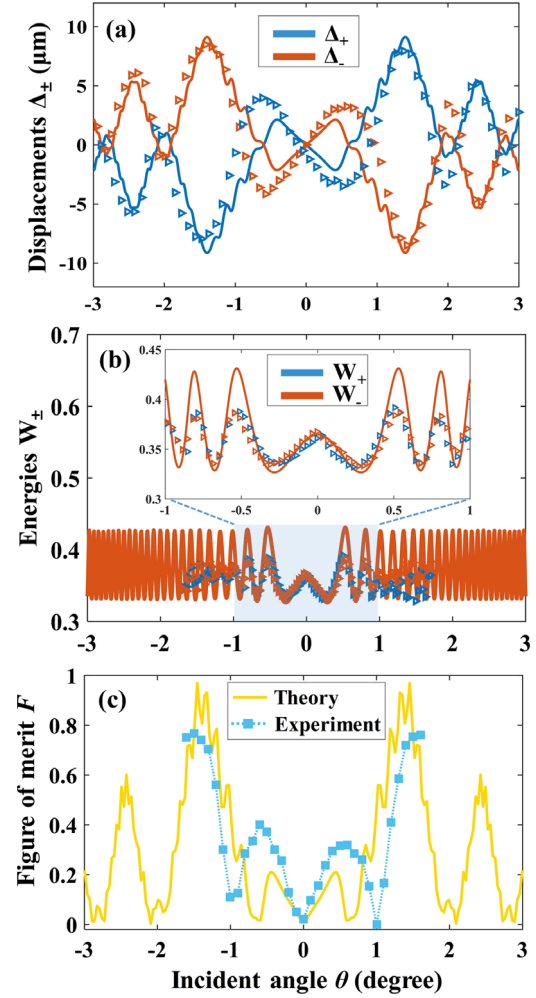

FIG. 4. Spin-dependent displacements (a), energies (b), and figures of merit (c) of the transmitted beam. Lines stand for theoretical prediction, whereas dots represent experiment results.

efficiency. As shown in Fig. 4(b), the theoretically predicted and experimentally measured total transmittances ($W_+ + W_-$) at $\theta = \pm1.40°$ are 66.2% and ~69.5%, respectively. The experimentally transmitted energies are not shown for $|\theta| > 1.6°$, since their rapid changes at $|\theta| > 1.6°$ will reduce the measurement accuracy. The maximum total transmission ($W_+ + W_-$) obtained in the experiment is 80%, slightly smaller than the theoretical prediction of 86%. The loss results from the reflection at the crystal surface due to the impedance mismatch. This can be overcome by coating the crystal with an antireflection film [32].

The spin separation with respect to the intensity spot size, $\tau = |\Delta|/w_0$, is a good parameter to quantify the separation of the intensity profiles of the two opposite-spin components; see Fig. 5(b). To make a comprehensive assessment of the PSHE, we introduce a figure of merit $F = (W_+ + W_-)\tau$. As shown in Fig. 4(c), the theoretically predicted maximum F is up to 0.97 at $\pm1.45°$, whereas the experimentally obtained maximum F is 0.77 at $\pm1.5°$. In contrast, for an

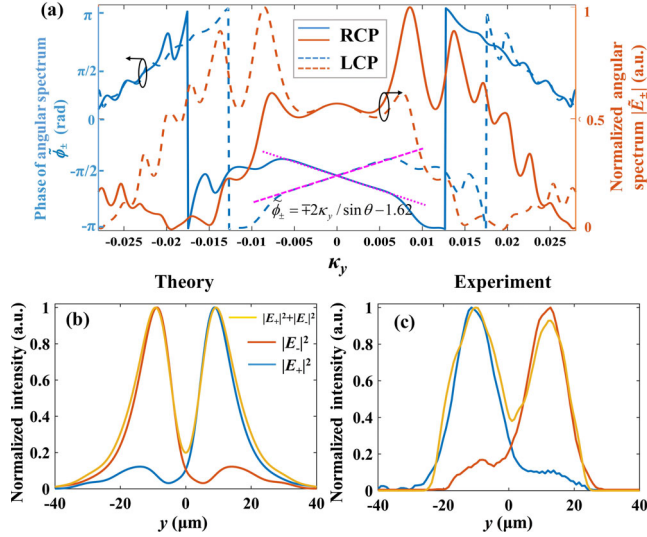FIG. 5. (a) Phase and amplitude of the angular spectrum of the transmitted RCP and LCP components for a beam waist of 7.5 μm and $\theta = 1.40°$. Theoretical (b) and experimental (c) normalized intensity profiles of the RCP and LCP components, and the total transmitted light field.

air-prism interface, F is only $\sim10^{-5}$ for H polarized Gaussian incident beams near the Brewster angle.

Figure 5(a) presents the phase and amplitude of the angular spectrum of the transmitted RCP and LCP components when $w_0 = 7.5$ μm and $\theta = 1.40°$. The spin-dependent linear PB phase can be clearly seen within the transverse wave vector range of $|\kappa_y| < 0.0065$, i.e., $\tilde{\phi}_\pm = \mp 2\kappa_y/\sin\theta - 1.62$.

The wave-vector-varying PB phase shifts the RCP and LCP components toward opposite directions. In coincidence with the prediction of Eq. (4), the spin-dependent displacements are $\Delta_\pm = \pm 8.3$ μm, leading to a spin separation of 16.6 μm, which is 2.2 times the incident beam waist. This large spin separation can split the two opposite-spin components completely, as shown in Figs. 5(b) and 5(c). The complete spin separation causes a theoretical dip of 0.19 at the middle of the total intensity profile in comparison with the experimental value of 0.39. The energy efficiency (total transmittance) reaches 70% with the figure of merit being $F = 1.54$.

Finally, we investigated the novel PSHE for two-dimensional (2D) Gaussian beams. For 2D beams, the angular dispersion of the transmission coefficients must be considered, which is supposed to reduce the spin separation compared with the 1D case. By replacing the cylindrical lens pair by a spherical lens pair with the same focal length ($f = 50$ mm), we measured the spin-dependent displacements, and the results are shown in Fig. 6(a). The maximum spin separation 12.0 μm is obtained at $\theta = \pm 1.1°$, which is smaller than that for the 1D incident beam. F is measured to be ~ 0.42. The theoretical and experimental intensity profiles are shown in Fig. 6(b) for incident angles of $\theta = 0, \pm 0.6°$, and $\pm 1.2°$. The spin-dependent movements
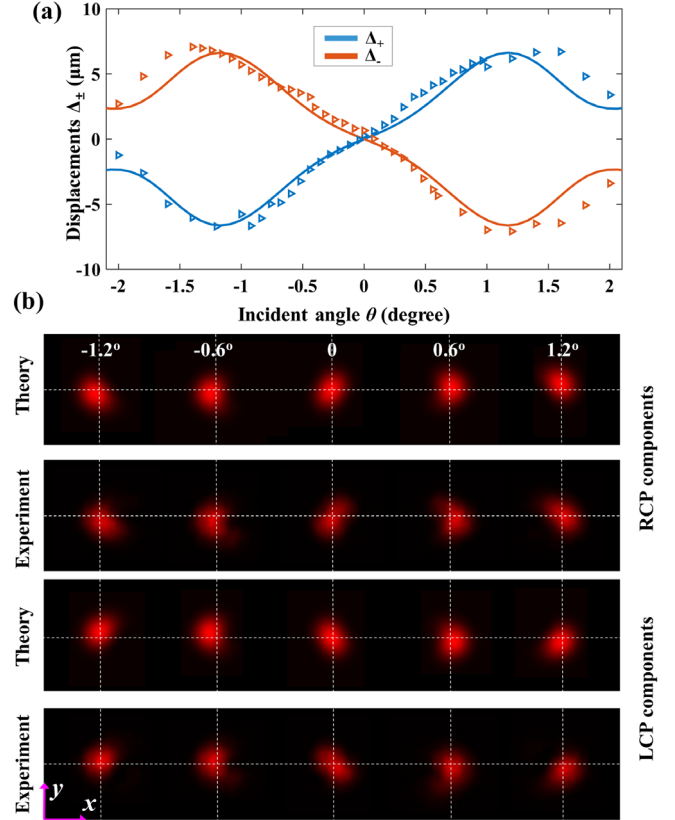

FIG. 6. (a) Change of spin-dependent displacements with the incident angle for 2D paraxial light beams. (b) Comparison of theoretical and experimental intensity profiles for different incident angles.

are along the y axis, in addition to the spin-independent movements along the x axis.

The PSHE was also examined by propagating RCP and LCP light beams into the crystal subsequently. As shown in Fig. S6 in Supplemental Material [32], the intensity profiles of the total transmitted fields are in "u" and "n" shapes for RCP and LCP incident states, respectively, revealing the spin-dependent centroid movements. The change of the intensity profiles with the incident polarization state is visualized in the supplemental video.

Bliokh et al. [40] studied the PSHE of transmitted light beams through a tilted half-wave plate, an optical system having strong in-plane anisotropy. They attributed the PSHE to the "circular birefringence" of the crystal plates and measured the nanoscale spin-dependent displacements by a weak measurement technique [40]. Here, we have achieved larger spin separations with high energy efficiencies with the assistance of the novel wave-vector-varying PB phase, which arises when light beams are launched almost normally to a uniaxial crystal with its optical axis perpendicular to the interface.

In conclusion, a novel PSHE based on the wave-vector-varying PB phase has been proposed and demonstrated. This PB phase is shown to arise naturally in the reflection

and transmission processes for paraxial beams with a small incident angle without the need for spatially inhomogeneous anisotropic media. By transmitting a 1D paraxial Gaussian beam through a uniaxial YVO_3 crystal at $\theta = 1.40°$, the opposite-spin photons can be completely separated with a spin separation of 16.6 μm ($2.2w_0$) and a high energy efficiency of $\sim 70\%$, breaking the upper limit of the spin separation in the conventional PSHE. The figure of merit of the novel PSHE can reach 1.54, 5 orders of magnitude larger than that of the conventional PSHE. For 2D incident beams, the figure of merit can be 0.58. The dynamic of spin separation in the uniaxial crystal is analyzed with wave coupling equations. For RCP and LCP incident states, the centroid positions of the spin photons can be doubled. These findings not only deepen our understanding in the geometric phase and spin-orbit coupling, but also open a new avenue to manipulate spin photons by the wave-vector-varying PB phase.

[*]Corresponding author.
zhuwg88@163.com
[†]kensomyu@gmail.com

[1] E. Cohen, H. Larocque, F. Bouchard, F. Nejadsattari, Y. Gefen, and E. Karimi, Nat. Rev. Phys. 1, 437 (2019).
[2] Y.-H. Lee, G. Tan, T. Zhan, Y. Weng, G. Liu, F. Gou, F. Peng, N. V. Tabiryan, S. Gauza, and S.-T. Wu, Opt. Data Process. Storage 3, 79 (2017).
[3] M. V. Berry, Proc. R. Soc. A 392, 45 (1984).
[4] S. Pancharatnam, Proc. Indian Acad. Sci. A. 44, 398 (1956).
[5] K. Y. Bliokh, Y. Gorodetski, V. Kleiner, and E. Hasman, Phys. Rev. Lett. 101, 030404 (2008).
[6] M. Tymchenko, J. S. Gomez-Diaz, J. Lee, N. Nookala, M. A. Belkin, and A. Alù, Phys. Rev. Lett. 115, 207403 (2015).
[7] E. Karimi, S. A. Schulz, I. De Leon, H. Qassim, J. Upham, and R. W. Boyd, Light 3, e167 (2014).
[8] X. Zhang, S. Yang, W. Yue, Q. Xu, C. Tian, X. Zhang, E. Plum, S. Zhang, J. Han, and W. Zhang, Optica 6, 1190 (2019).
[9] W. Luo, S. Sun, H. X. Xu, Q. He, and L. Zhou, Phys. Rev. Applied 7, 044033 (2017).
[10] X. Ling, X. Zhou, X. Yi, W. Shu, Y. Liu, S. Chen, H. Luo, S. Wen, and D. Fan, Light 4, e290 (2015).
[11] Y. He, Z. Xie, B. Yang, X. Chen, J. Liu, H. Ye, X. Zhou, Y. Li, S. Chen, and D. Fan, Photonics Res. 8, 963 (2020).
[12] R. Barboza, U. Bortolozzo, M. G. Clerc, and S. Residori, Phys. Rev. Lett. 117, 053903 (2016).
[13] M. Pal, C. Banerjee, S. Chandel, A. Bag, S. K. Majumder, and N. Ghosh, Sci. Rep. 6, 39582 (2016).
[14] Z. Zhang, H. Liang, T. He, Z. Wang, and X. Cheng, Appl. Opt. 59, A63 (2020).
[15] K. Y. Bliokh, F. J. Rodríguez-Fortuño, F. Nori, and A. V. Zayats, Nat. Photonics 9, 796 (2015).
[16] H. Dai, L. Yuan, C. Yin, Z. Cao, and X. Chen, Phys. Rev. Lett. 124, 053902 (2020).
[17] O. Hosten and P. Kwiat, Science 319, 787 (2008).
[18] X. Yin, Z. Ye, J. Rho, Y. Wang, and X. Zhang, Science 339, 1405 (2013).
[19] M. Onoda, S. Murakami, and N. Nagaosa, Phys. Rev. Lett. 93, 083901 (2004).
[20] K. Y. Bliokh and A. Aiello, J. Opt. 15, 014001 (2013).
[21] Y. Qin, Y. Li, H. He, and Q. Gong, Opt. Lett. 34, 2551 (2009).
[22] H. Luo, X. Zhou, W. Shu, S. Wen, and D. Fan, Phys. Rev. A 84, 043806 (2011).
[23] H. Lin, M. Jiang, L. Zhuo, W. Zhu, H. Guan, J. Yu, H. Lu, J. Tan, J. Zhang, and Z. Chen, Opt. Commun. 431, 136 (2019).
[24] Y. Xiang, X. Jiang, Q. You, J. Guo, and X. Dai, Photonics Res. 5, 467 (2017).
[25] W. Xu, Q. Yang, G. Ye, W. Wu, W. Zhang, H. Luo, and S. Wen, Phys. Rev. A 101, 023826 (2020).
[26] W. Zhu and W. She, Opt. Lett. 40, 2961 (2015).
[27] W. Zhu, J. Yu, H. Guan, H. Lu, J. Tang, J. Zhang, Y. Luo, and Z. Chen, Sci. Rep. 7, 1150 (2017).
[28] X. Qiu, L. Xie, X. Liu, L. Luo, Z. Zhang, and J. Du, Opt. Lett. 41, 4032 (2016).
[29] W. Zhu, J. Yu, H. Guan, H. Lu, J. Tang, Y. Luo, and Z. Chen, Opt. Express 25, 5196 (2017).
[30] W. Long, J. Pan, X. Guo, X. Liu, H. Lin, H. Zheng, J. Yu, H. Guan, H. Lu, Y. Zhong, S. Fu, L. Zhang, W. Zhu, and Z. Chen, Photonics Res. 7, 1273 (2019).
[31] J. L. Ren, B. Wang, Y. F. Xiao, Q. Gong, and Y. Li, Appl. Phys. Lett. 107, 111105 (2015).
[32] See Supplemental Material at http://link.aps.org/supplemental/10.1103/PhysRevLett.126.083901 for detailed derivations of the spin-dependent displacements and wave coupling equations, discussions of the spin-orbit coupling in uniaxial crystal, the spin-dependent displacements vs L, and the PSHE at the interface between air and metamaterial, a detailed comparison of spin separation for the bare crystal and the crystal coated with antireflection films, and an examination of the PSHE with RCP and LCP incident states, which includes Refs. [33].
[33] A. Alù, M. G. Silveirinha, A. Salandrino, and N. Engheta, Phys. Rev. B 75, 155410 (2007).
[34] L. Marrucci, C. Manzo, and D. Paparo, Phys. Rev. Lett. 96, 163905 (2006).
[35] A. Ciattoni, G. Cincotti, D. Provenziani, and C. Palma, Phys. Rev. E 66, 036614 (2002).
[36] K. Rechcinska, M. Król, R. Mazur, P. Morawiak, R. Mirek, K. Łempicka, W. Bardyszewski, M. Matuszewski, P. Kula, W. Piecek, P. G. Lagoudakis, B. Pietka, and J. Szczytko, Science 366, 727 (2019).
[37] A. Manchon, H. C. Koo, J. Nitta, S. M. Frolov, and R. A. Duine, Nat. Mater. 14, 871 (2015).
[38] K. Rong, B. Wang, A. Reuven, E. Maguid, B. Cohn, V. Kleiner, S. Katznelson, E. Koren, and E. Hasman, Nat. Nanotechnol. 15, 927 (2020).
[39] S. Fu, C. Guo, G. Liu, Y. Li, H. Yin, Z. Li, and Z. Chen, Phys. Rev. Lett. 123, 243904 (2019).
[40] K. Y. Bliokh, C. T. Samlan, C. Prajapati, G. Puentes, N. K. Viswanathan, and F. Nori, Optica 3, 1039 (2016).